SELF-EXCITED COMPRESSIBLE PLANAR MIXING LAYERS AT ARBITRARY MACH NUMBERS: NUMERICAL OR PHYSICAL PHENOMENA?

Renan de S. Teixeira, renanpcivil@yahoo.com.br
Programa de Pós-Graduação em Engenharia de Defesa
Leonardo S. de B. Alves, leonardo_alves@ime.eb.br
Laboratório de Motores e Propulsão, Departamento de Engenharia Mecânica e de Materiais, Instituto Militar de Engenharia, Praia Vermelha 80, Rio de Janeiro, RJ 22290-270, Brazil.

Abstract. *Unsteady simulations of planar mixing layers are usually started using approximate solutions, obtained from a hyperbolic tangent function or boundary-layer equations, as initial conditions. This choice introduces large disturbances during the first time step, causing a phenomenon that is known in the literature as start-up vortex. The amplitude of this vortex increases significantly when the velocity ratio and/or the faster stream Mach number increase. It has been suggested that its origin is a first derivative discontinuity between initial and inflow boundary conditions. However, it is shown in the present work that this is actually caused by a mismatch between initial and outflow boundary conditions instead. This is demonstrated through the use of a high accuracy reference solution as initial condition and also buffer region for global boundary conditions at both inflow and outflow artificial boundaries.*

Keywords: *Start-up Vortex, Hydrodynamics Stability, Planar Mixing-layers, Initial and Boundary Conditions.*

1. INTRODUCTION

A planar mixing layer is formed when two streams with different speeds meet downstream of a splitter plate. This configuration represents a free shear layer that is convectively unstable for very low Reynolds numbers and constant properties. In such cases, small perturbations are amplified as they propagate downstream. However, the transition to a globally unstable flow can occur due to temperature changes or when the layers move in opposite directions.

Numerical simulations of external flow problems pose one of the most difficult challenges in computational fluid dynamics because the original unbounded domain must be limited to a bounded one. This difficulty stems from the need for artificial initial and, more importantly, boundary conditions. The first coherent structure formed in a transient simulation of planar mixing layers is the startup vortex. A first derivative discontinuity between initial and inflow conditions has been deemed responsible for its formation (Buell and Huerre, 1988). In the absence of external excitations, the flow should relax to its steady-state solution according to both linear (Huerre and Monkewitz, 1990) and nonlinear (Chomaz, 2005) stability analyzes. As expected from a convectively unstable flow, the initial vortex amplitude increases as it propagates downstream. However, a new vortex is excited near the inflow whenever another one reaches the outflow boundary. This numerical reflection between inflow and outflow boundary conditions may become self-sustained, forming an artificial global instability.

The small amount of computer simulations about this problem present in the literature can be seen in the article by McMullan *et al.* (2007), which simulates incompressible spatially developing planar mixing layers in two and three dimensions. The hyperbolic tangent function and data derived from boundary layer simulations are used to generate the inflow conditions, which are extended to the rest of the domain in order to form the respective initial conditions. They show important differences between each one of these cases, providing strong evidence that initial conditions must be as close as possible to the experiment they intend to reproduce for a good agreement to be possible.

Nevertheless, some authors have claimed otherwise. Grinstein *et al.* (1990) used the conservative compressible flow equations to simulate spatially planar mixing layers. At the inflow boundary, all variables were prescribed except pressure, which was obtained from a zero gradient condition. On the other hand, linear advection equations were imposed using the local velocity near the outflow boundary, where pressure was relaxed towards a specified ambient value. Initial and inflow velocity profiles were defined using a hyperbolic tangent function. In order to avoid numerical reflections at the boundaries, simulations were performed on a long very domain and restricted to small enough times, not allowing any of the vortexes formed to reach the boundaries. These authors conclude that downstream pressure gradients due to vortex pairing affect the formation of these vortices upstream. They also state that this effect is reduced when: 1) the propagation speed of pressure waves in each stream tends to be equal, i.e., at the incompressible limit, and 2) the free stream convective velocities os each layer tends to be equal. This study was repeated by Grinstein and DeVore (2002) for free coaxial jets, where the inner jet is supersonic ant the outer jet is subsonic and moves in an opposite direction. The self-excitation occurs in this case due to subsonic speed of the external annular jet , despite the supersonic speed of the internal one. A review of these results can be found in the article by Drikakis *et al.* (2005).

The major problem of these studies lies in the quality of the initial and boundary conditions used in both compressible and incompressible simulations. The best boundary conditions for artificial boundaries found in the literature today are the

ones used in compressible flow simulations (Colonius, 2004), since incompressible flows do not account for characteristics propagation directions (Poinsot and Lele, 1992). The challenge then is to extend the use of these boundary conditions for incompressible mixing layers. This study is an extension of previously reported work by Teixeira *et al.* (2008) as well as Teixeira and Alves (2010). It investigate the influence of initial and artificial boundary conditions in the computer simulation of unsteady compressible planar mixing layers.

2. GOVERNING EQUATIONS

The two-dimensional preconditioned governing equation are

$$\mathbf{\Gamma}\frac{\partial\hat{\mathbf{Q}}}{\partial\tau}+\frac{\partial\mathbf{Q}}{\partial t}+\frac{\partial}{\partial x}(\mathbf{E}_i-\mathbf{E}_v)+\frac{\partial}{\partial y}(\mathbf{F}_i-\mathbf{F}_v)=\mathbf{H} \tag{1}$$

where the set of variables $\hat{\mathbf{Q}}$ and $\mathbf{Q}$ are given by transpose vectors below

$$\hat{\mathbf{Q}}=(p_g,u,v,T,Y_1)^T \quad \text{and} \quad \mathbf{Q}=(\rho,\rho u,\rho v,\rho E,\rho Y_1)^T, \tag{2}$$

with ρ standing for density, p for pressure, u and v for the Cartesian velocity components, e for thermal internal energy, $E=e+(u^2+v^2)/2$ for total internal energy, Y_1 for mass fraction of specie 1 and N for the total number of species in the mixture, where $N=2$ here. The inviscid and viscous fluxes $\mathbf{E}_i$, $\mathbf{E}_v$, $\mathbf{F}_i$ e $\mathbf{F}_v$ have a standard definition and $\mathbf{H}$ represents the source term. More details about the preconditioned differential model used here is provided by Teixeira *et al.* (2008) and further information about the numerical schemes employed are given by Teixeira and Alves (2010).

2.1 Boundary Conditions

One of the critical points in the computer simulation of external flows is the appropriate implementation of boundary conditions. A possible solution to this problem is coordinate transformation, i.e., mapping the unbounded domain into a bounded one before attempting a numerical solution of the respective governing equations (Grosch and Orszag, 1977). However, the loss of implicit mesh resolution introduces undesirable numerical oscillations whenever the flow does not relax smoothly to its boundary conditions at infinity. Hence, truncation of the infinite or semi-infinite domain is necessary, which creates an artificial boundary where approximate conditions must be imposed instead of the original conservation equations. Unfortunately, these additional approximations can generate undesirable numerical reflections.

Two types of high accuracy artificial boundary conditions can be found in the literature mitigate this problem. The first type includes global boundary conditions, which require a finite region that extends away from the boundary to damp any errors generated by its artificial condition (Blaschak and Kriegsmann, 1988; Bodony, 2006). Stretched meshes, commonly used to introduce dissipation in the far field, can be considered a subset of this group. However, arguably the most widely used method is known as a buffer zone. This method introduces a source term in the conservation equations that forced the computed solution towards a reference solution within a predefined region near the artificial boundary. Thus, undesirable oscillations are damped before reaching the boundary. The other type is known as local boundary conditions, since it only acts on the line (2D) or surface (3D) of the artificial boundary. One of the most used techniques is known as non-reflective boundary conditions, which models the behavior of linear perturbations around a base flow (Giles, 1990; Colonius *et al.*, 1993). Another widely known technique is referred to as method of characteristics (Thompson, 1987; Poinsot and Lele, 1992). This method prevents characteristic wave coming from outside the truncated domain to enter it, minimizing unwanted numerical reflections.

The original code by Teixeira *et al.* (2008) works with a local boundary condition that uses a version of the method of characteristics known as *LODI* (Poinsot and Lele, 1992). This technique is discussed bellow with an important improvement used by Teixeira and Alves (2010) and described here in detail. Global boundary conditions have also been implemented, discussed and shown for the first time in the present work.

2.1.1 Local Boundary Condition

An appealing technique used to specify boundary conditions for hyperbolic systems is based on characteristic lines' relations, i.e., on the analysis of the different waves crossing the boundary. This method, called L.O.D.I. in the litrature, has been extensively studied and is based on local Euler equations normal to the boundary (Poinsot and Lele, 1992). It determines the direction of propagation of the convective and acoustic waves at the boundary, filtering the waves that are entering the domain (Thompson, 1987).

First, consider the Euler equations below

$$\frac{\partial\mathbf{Q}}{\partial t}+\frac{\partial\mathbf{E}_i}{\partial x}=0 \tag{3}$$

where $\mathbf{Q}$ is the vector of conservative variables and $\mathbf{E}_i$ vector of inviscid fluxes (Teixeira and Alves, 2010). By applying

the chain rule in equation (3), the following equation is obtained

$$\frac{\partial \mathbf{Q}}{\partial t} + \frac{\partial \mathbf{E}_i}{\partial \mathbf{Q}} \frac{\partial \mathbf{Q}}{\partial x} = 0 \quad \text{or} \quad \frac{\partial \mathbf{Q}}{\partial t} + \mathbf{A} \frac{\partial \mathbf{Q}}{\partial x} = 0, \tag{4}$$

where it is defined that $\mathbf{A} = \partial \mathbf{E}_i / \partial \mathbf{Q}$.

Using the right eigenvector matrix $\mathbf{M}$ to diagonalize matrix $\mathbf{A}$ leads to

$$\mathbf{M}^{-1} \frac{\partial \mathbf{Q}}{\partial t} + (\mathbf{M}^{-1} \mathbf{A} \mathbf{M}) \mathbf{M}^{-1} \frac{\partial \mathbf{Q}}{\partial x} = 0, \tag{5}$$

which can also be written as

$$\frac{\partial \omega}{\partial t} + \mathbf{\Lambda} \frac{\partial \omega}{\partial x} = 0, \tag{6}$$

if the following relations are defined

$$\frac{\partial \omega}{\partial t} = \mathbf{M}^{-1} \frac{\partial \mathbf{Q}}{\partial t} \quad \text{and} \quad \frac{\partial \omega}{\partial x} = \mathbf{M}^{-1} \frac{\partial \mathbf{Q}}{\partial x}, \tag{7}$$

where $\mathbf{\Lambda}$ is the eigenvalue matrix of $\mathbf{A}$ given by

$$\mathbf{\Lambda} = \mathbf{M}^{-1} \mathbf{A} \mathbf{M} = \begin{pmatrix} \lambda_1 & 0 & 0 \\ 0 & \lambda_2 & 0 \\ 0 & 0 & \lambda_3 \end{pmatrix}. \tag{8}$$

System of equations (5) is orthogonal, where each equation, written as

$$\frac{\partial \omega_1}{\partial t} + \lambda_1 \frac{\partial \omega_1}{\partial x} = 0 \quad , \quad \frac{\partial \omega_2}{\partial t} + \lambda_2 \frac{\partial \omega_2}{\partial x} = 0 \quad \text{and} \quad \frac{\partial \omega_3}{\partial t} + \lambda_3 \frac{\partial \omega_3}{\partial x} = 0 \quad , \tag{9}$$

can be solved separately, where the eigenvalues λ_i are given by

$$\lambda_1 = u \quad , \quad \lambda_2 = u + c \quad \text{and} \quad \lambda_3 = u - c \quad , \tag{10}$$

and the characteristics ω_i are given by

$$\omega_1 = s \quad , \quad \omega_2 = u + \frac{2}{\gamma - 1} c \quad \text{and} \quad \omega_3 = u - \frac{2}{\gamma - 1} c \quad , \tag{11}$$

where s is entropy and γ the ratio between specific heats.

According to characteristic propagation directions, given by the eigenvalues above, a boundary condition implementation procedure is defined in Table (1). Since subsonic inflow and outflow conditions are used in the present work, ω_1 and ω_2 are fixed and ω_3 is calculated at the inlet , whereas ω_1 and ω_2 are calculated and ω_3 is fixed at the outlet. Once the appropriate wave crossing the boundary is removed from the orthogonal system, the procedure is reversed, leading to a filtered version of the original Euler equations. An improved version of this approach is considered in the present paper, where the inviscid and viscous terms tangent to the artificial boundary are added back into the filtered Euler equations. As will be seen later, this simple additional procedure greatly increases boundary condition accuracy.

The prescribed conditions used at the inlet are

$$u(0, y) = \bar{U} \left(1 + R \tanh \left[\frac{y}{2\theta_0} \right] \right) \quad \text{and} \quad v(0, y) = 0, \tag{12}$$

where $R = \Delta U / (2\bar{U})$ is the ratio between velocity difference $\Delta U = U_2 - U_1$ and mean velocity $\bar{U} = (U_1 + U_2)/2$, and θ_0 is the momentum thickness. On the other hand, only pressure is prescribed at the outlet:

$$p(1, y) = p_{atm}. \tag{13}$$

	Subsonic	Supersonic
Inlet	Two conditions (ω_1 and ω_2)	Three conditions (ω_1, ω_2 and ω_3)
Outlet	One condition (ω_3)	No conditions

Table 1. Numbers of prescribed boundary conditions according to $LODI$

2.1.2 Global Boundary Condition

Absorbing conditions, a subset of global boundary conditions (Colonius, 2004), are conditions where the physics of the problem is modified in a finite region of the flow. This region can be located anywhere within the flow domain. Given the compressible Navier-Stokes equations (Teixeira and Alves, 2010), a source term is introduced as follows

$$\frac{\partial \mathbf{Q}}{\partial t} + \frac{\partial}{\partial x}(\mathbf{E}_i - \mathbf{E}_v) + \frac{\partial}{\partial y}(\mathbf{F}_i - \mathbf{F}_v) = -\sigma(\mathbf{Q} - \mathbf{Q}_0) \tag{14}$$

where $\mathbf{Q_0}$ is a reference solution and σ controls the buffer region and was chosen according to Freund (1997),

$$\sigma(x) = \begin{cases} \sigma_o \left(\dfrac{W_\sigma - x}{W_\sigma} \right)^\beta & ; \quad 0 \leq x < W_\sigma \\ 0 & ; \quad W_\sigma \leq x < W_\sigma - x_{max} \\ \sigma_o \left(\dfrac{x - (x_{max} - W_\sigma)}{W_\sigma} \right)^\beta & ; \quad x_{max} - W_\sigma \leq x < x_{max} \end{cases} \tag{15}$$

where W_σ is the buffer zone length, x_{max} is the computational domain length and σ_o is an arbitrary constant that controls the absorption levels. This parameter must be much larger than the other terms in the governing equations, including inviscid and viscous fluxes, in order to allow the numerical solution to smoothly converge towards the reference solution.

3. RESULTS AND DISCUSSION

This study begins with planar mixing layer simulations ran using standard initial conditions, i.e., hyperbolic tangent function for the streamwise velocity, zero for the transverse velocity and imposed atmospheric pressure and temperature. Furthermore, the standard *LODI* formulation discussed at the end of subsection 2.1 was used at the inflow and outflow artificial boundaries (Teixeira *et al.*, 2008). The mesh used is described in Teixeira and Alves (2010), where free-stream velocities are $U_1 = 0.34605\ m/s$ e $U_2 = 0.173025\ m/s$. Figure 1 shows the transverse velocity disturbance behavior in time, obtained by subtracting the steady-state solution from the unsteady simulation results. All curves were measured at the shear-layer centerline, with each consecutive curve located one wavelength downstream of the previous one, starting one wavelength downstream of the inlet. This wavelength was obtained from the most amplified perturbation according to linear stability theory. The numbers in each line show the maximum amplitude of each wave. Based on this figure, it seems there is a perturbation at the inlet during the initial transient. Its amplitude increases as it is propagated downstream by the mean flow, a clear indication of a convective instability. This is the start-up vortex, also observed in Figure 2, which shows streamwise velocity disturbance isolines from the same simulation at four different times. It does seem likely that this coherent structure was generated by some type of perturbation due to a mismatch between initial and inlet conditions, a hypothesis originally stated by Buell and Huerre (1988).

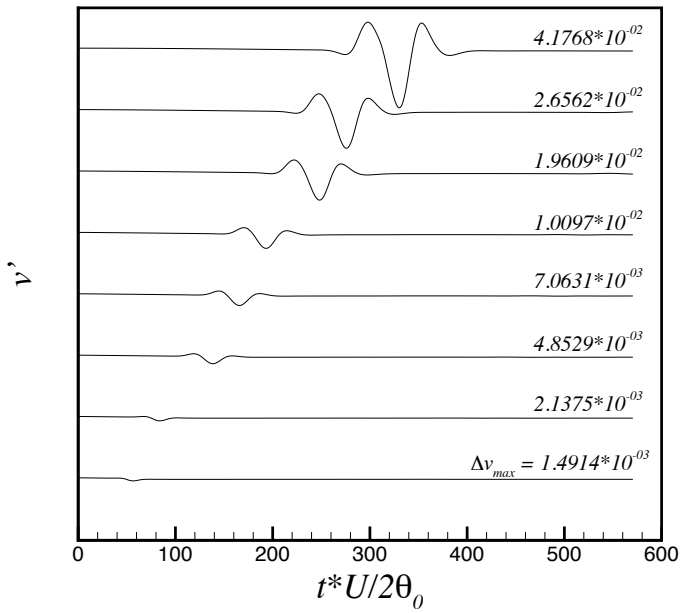

Figure 1. Transverse velocity disturbance obtained with standard LODI and tanh initial condition.

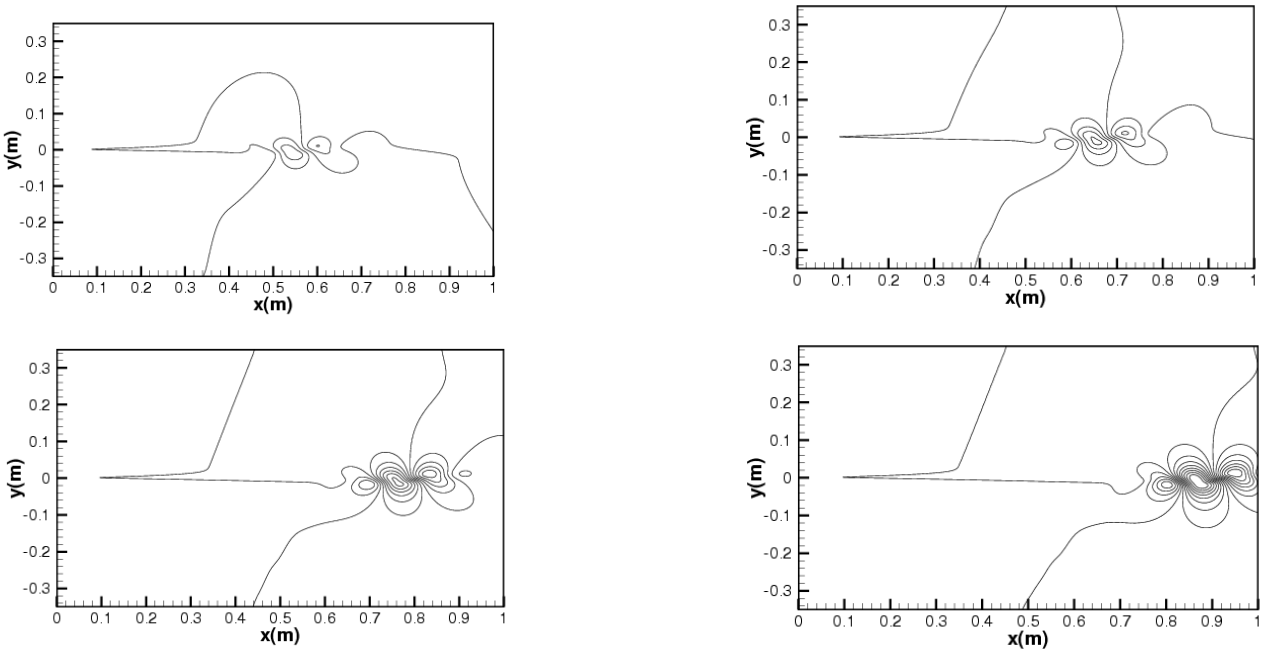

Figure 2. Streamwise velocity disturbance isolines from Figure 1 at times $t = 1.74s$, $2.17s$, $2.61s$ e $3.04s$.

3.1 Local Boundary Conditions

In an attempt to minimize this effect, the standard *LODI* inflow and outflow boundary conditions were modified to enhance their accuracy. As described previously, this boundary condition is based on the one-dimensional Euler equations normal to the artificial boundary. Its modified version simply adds to the filtered version of this equation any terms that are tangential to the artificial boundary. Two variations are considered here. The first one, called inviscid *LODI*, re-introduces only the tangential inviscid fluxes in the filtered equation. On the other hand, the second variation, called viscous *LODI*, introduces tangential inviscid and viscous fluxes.

Figures 3 and 4 show results from a simulation ran with the same conditions used to generate Figure 1, but using instead the inviscid and viscous *LODI* boundary conditions, respectively, at both inflow and outflow boundaries. The same qualitative behavior observed in Figure 1 is also seen in these Figures. Furthermore, the difference in transverse velocity disturbance amplitudes at any given downstream location between these figures is less than ten percent, even though the modified boundary conditions are supposed to greatly improve accuracy. This analysis indicates that there is another error source contaminating the numerical simulation, preventing any improvements these modified boundary conditions might otherwise yield. A possible candidate is the initial condition.

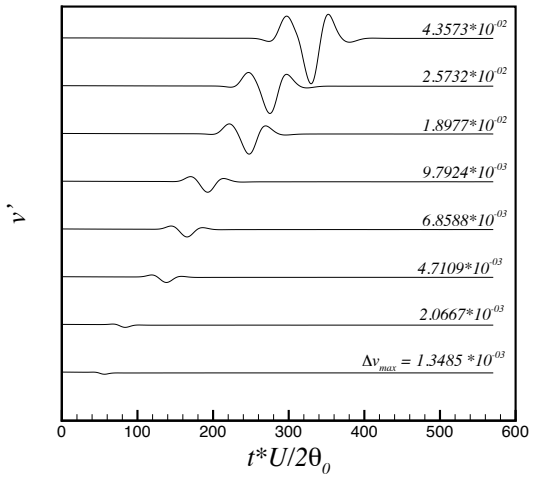

Figure 3. Transverse velocity disturbance obtained with inviscid LODI and tanh initial condition.

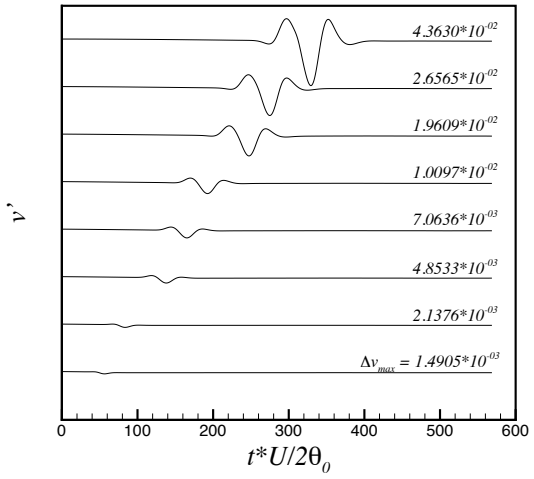

Figure 4. Transverse velocity disturbance obtained with viscous LODI and tanh initial condition.

Recent simulations of spatially periodic mixing layers using the boundary layer similarity profile as initial condition showed high-frequency oscillations in the unsteady solution (Lardjane *et al.*, 2004). This problem was minimized by modifying the similarity solution to account for spatial periodicity. Such an approach does show the impact of poorly chosen initial conditions, but cannot be extended to general problems. This modest gain in accuracy and lack of generality illustrates the need for new procedures that generate accurate reference solutions. An interesting alternative would be to use a steady state solution as initial condition. However, as is often the case, this solution is unstable. Hence, such a procedure must damp all unsteady disturbances without affecting spatial resolution. The best way to achieve this goal is to introduce dissipation through the transient term, since it disappears at steady state. Time marching with the Euler method was chosen here because it introduces a significant amount of dissipation. It is implemented in an implicit way to allow larger time steps, since its dissipation is proportional to the time step. Furthermore, time marching must be implemented in residual form to avoid time step dependent steady states (Tannehill *et al.*, 1997). Finally, it is important to remember that these steady states are artificial, since the flow is unstable. They are used only as initial conditions to minimize errors, since they also satisfy the steady part unsteady of the code (Teixeira and Alves, 2010).

New simulations were run with same conditions used to generate Figures 1, 3 and 4, but using their respective steady states as initial conditions instead. Their results are shown in Figures 5, 6 and 7, respectively. Now, the error introduced by the initial condition has been reduced dramatically and the largest source of error in the simulation are the boundary conditions. The amplitudes of the reflected waves near the outflow boundary, compared with their respective values obtained with the tanh initial condition, were approximately 25 times smaller with standard *LODI*, 558 times smaller with inviscid *LODI* and 546 times smaller with viscous *LODI*. These results confirm the expected greater accuracy of the modified *LODI* boundary conditions. More importantly, they demonstrate the importance of using accurate initial conditions in unsteady simulations.

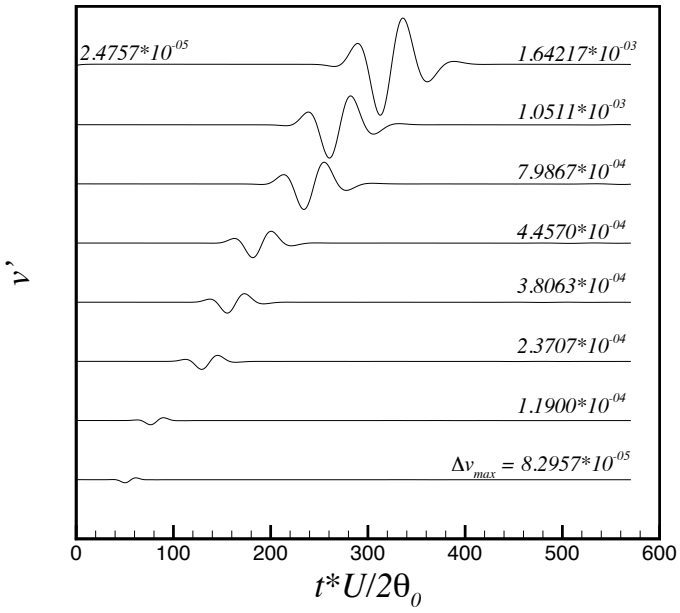

Figure 5. Transverse velocity disturbance obtained with standard LODI and steady state initial condition.

Now that the largest sources of error are the boundary, instead of initial, conditions, another important result can be seen in these figures. The origin of the start-up vortex has, for a long time, been attributed to a first derivative discontinuity between initial and boundary conditions at the inlet (Buell and Huerre, 1988), caused by the use of approximate initial conditions such as a hyperbolic tangent function or a similarity solution of the boundary layer equations. However, Figures 6 and 7, and to a smaller extent also Figure 5, show a small perturbation at very early times near the outflow boundary. In these figures, its amplitude is more than twice as large as the amplitude of the reflected wave near the inflow boundary. This is a strong indication that the start-up vortex is formed by a discontinuity between initial and outflow boundary conditions, since this perturbation travels upstream at the speed of sound in the form of pressure waves. Hence, the well known numerical self-excitation mechanism induced by inaccurate outflow boundary conditions is also responsible for the very first vortex formed in an unsteady simulation. This result is important because many studies found in the literature construct their initial conditions by extending whatever profiles are imposed at the inflow boundary towards the inner domain (Grinstein *et al.*, 1990, 1991; Grinstein, 1994; Grinstein and DeVore, 2002; Drikakis *et al.*, 2005). Perhaps even more imporant, they claim that downstream vortex mergers generate pressure waves that propagate upstream to excite new vortices at the inflow boundary, even though linear (Ho and Huerre, 1984; Huerre and Monkewitz, 1990) and nonlinear (Chomaz, 2005) stability analyzes show there is no such self-excitation mechanism under the same flow conditions.

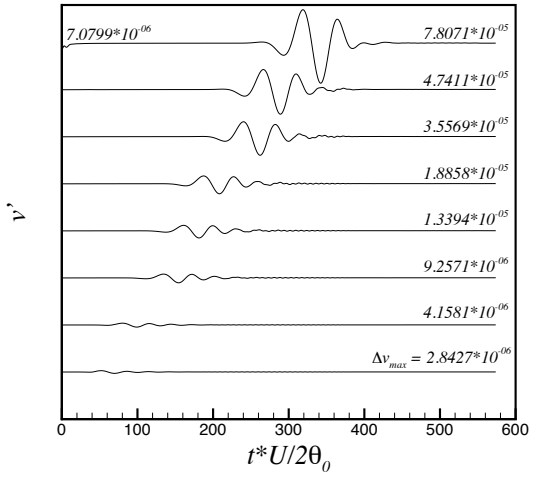

Figure 6. Transverse velocity disturbance obtained with inviscid LODI and steady state initial condition.

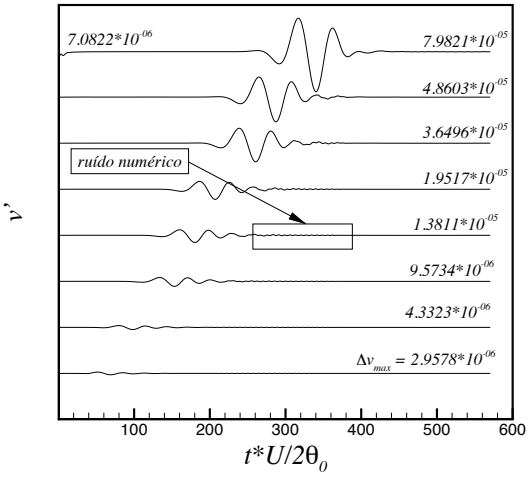

Figure 7. Transverse velocity disturbance obtained with viscous LODI and steady state initial condition.

3.2 Global Boundary Conditions

Additional evidence about the start-up vortex origins can be uncovered with the use of nonuniform meshes. They represent a well known technique that clusters grid points in regions with strong gradients as well as pushes artificial boundaries further away by stretching the distance between consecutive grid points. The former increases numerical accuracy whereas the latter introduces dissipation, damping perturbations crossing this region. It is considered a global boundary condition, since it utilizes a finite domain away from the boundaries (Colonius, 2004). Figures 8 and 9 show results from a simulation similar to the one performed to generate Figures 6 and 7, respectively. The difference between each group is the longitudinal grid point distribution. It is uniform in the second case, whereas points move away from each other monotonically from inflow to outflow in the first case. As one might expect, grid stretching increased the disturbance amplitude near the outflow boundary at very early times. Nevertheless, the reflected wave amplitude is still smaller because of the dissipative effect of a stretched mesh.

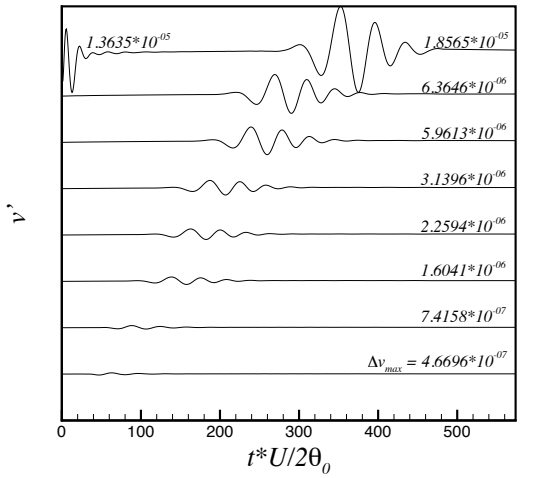

Figure 8. Same as Figure 6, but with a stretched mesh in the longitudinal direction.

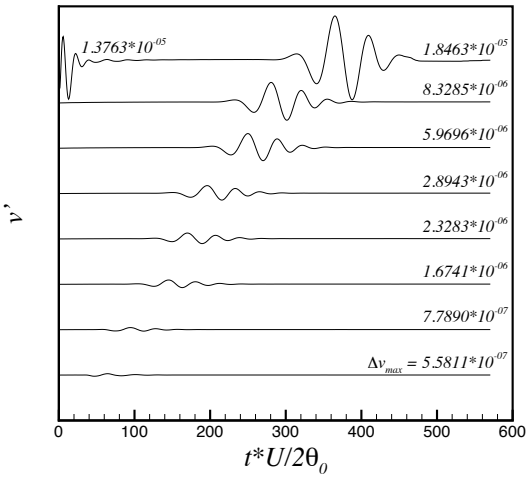

Figure 9. Same as Figure 7, but with a stretched mesh in the longitudinal direction.

Arguably the most effective way to minimize the effect of boundary generated numerical self-excitation is the use of buffers, also known as sponge zones or absorption regions, yet another type of global boundary conditions (Colonius and Lele, 2004; Wang *et al.*, 2006). This technique forces the simulation towards a reference solution within a predefined finite region of the domain, damping unwanted oscillations. When placed near artificial boundaries, it can be used to control numerical self-excitation. However, its strength and size must be carefully controlled, otherwise the buffer itself might reflect nonphysical numerical waves.These techniques have been successfully used to simulate flow generated sound in

many open shear flows (Colonius *et al.*, 1993; Freund, 1997; Freund *et al.*, 2000; Freund, 2001; Wei and Freund, 2005). It is interesting to note that in these simulations, placing a buffer near the inflow, instead of outflow, boundary was a more effective way to minimize numerical self-excitation.

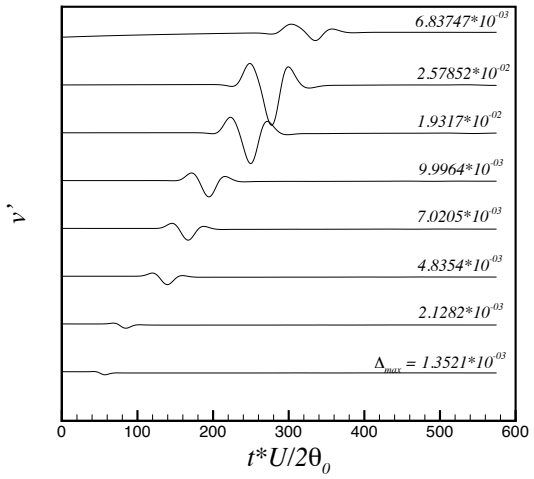

Figure 10. Same as Figure 4, but using an outflow buffer region with $\sigma_0 = 0.1$.

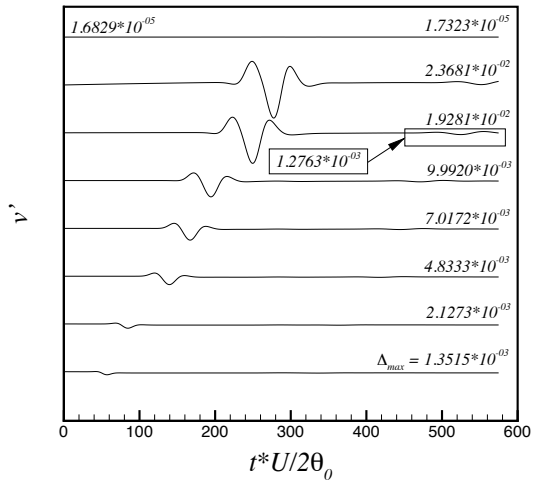

Figure 11. Same as Figure 4, but using an outflow buffer region with $\sigma_0 = 1.0$.

The next test placed a buffer region near the outflow boundary. Only results obtained with the viscous *LODI* boundary condition will be shown, since the inviscid *LODI* variant leads to similar results. Figures 10 and 11 do reproduce the simulation used to generate Figure 4, but now using absorption regions of different lengths. Two conclusions can be drawn from these figures. First, the outflow buffer has a small but non-negligible effect on the start-up vortex. However, if this coherent structure is generated by an inconsistency between inflow and initial conditions, the outflow buffer should have no effect whatsoever on this vortex structure. On the other hand, the buffer does reduce the inconsistency between outflow and initial conditions. Furthermore, this problem can still generate upstream moving pressure waves since it is already at the outflow boundary during the very first time step. Another evidence in favor of numerical self-excitation as the cause of the start-up vortex. Second, when the buffer strength is increased, a second reflected wave appears in the simulation. This is an expected result, but it should be noted that this new wave does have a much smaller amplitude. Figures 12 and 13 show results obtained when reproducing the simulation used to generate Figure 7, but now using absorption regions of different lengths. The same trends already discussed are observed once again.

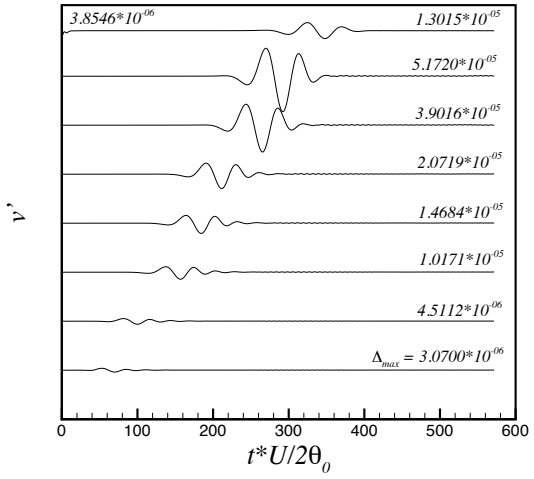

Figure 12. Same as Figure 7, but using an outflow buffer region with $\sigma_0 = 0.1$.

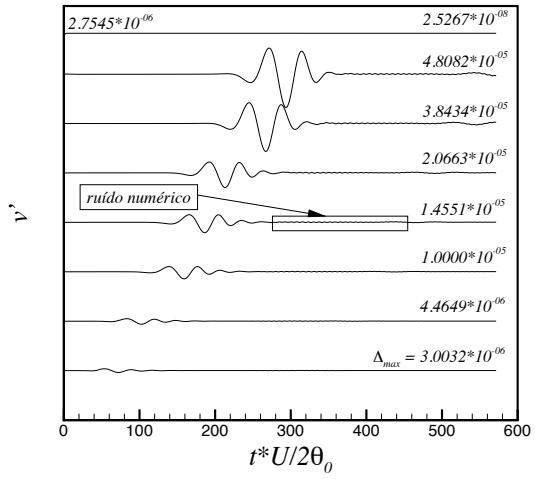

Figure 13. Same as Figure 7, but using an outflow buffer region with $\sigma_0 = 1.0$.

As a final test, the previous four simulations are repeated but now with a buffer placed near the inflow, instead of outflow, boundary. Figures 14 e 15 show a small decrease in the start-up vortex amplitude when compared to Figure 4. This is also true when they are compared to Figures 10 and 11, as expected. Another important difference and, hence, advantage for the inflow buffer, is the absence of a second reflected wave. These improvements are significantly more dramatic when a steady-state is used as reference solution for the inflow buffer, as can be seen in Figures 16 and

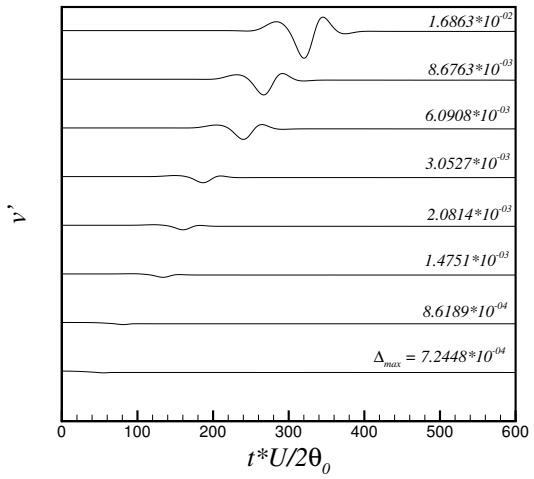

Figure 14. Same as Figure 4, but using an inflow buffer region with $\sigma_0 = 0.1$.

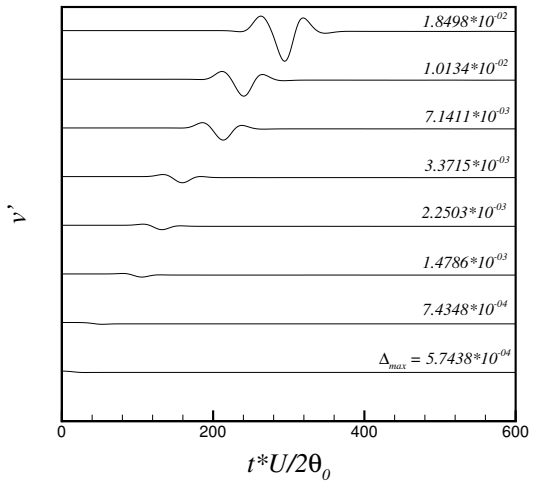

Figure 15. Same as Figure 4, but using an inflow buffer region with $\sigma_0 = 1.0$.

17. Numerical self-excitation is not present, even though the initial and outflow boundary inconsistency is still present. Reflected waves cannot be observed because they are smaller than the prescribed tolerance for the sub-iteration procedure used at each time step, which is $O(10^{-8})$ (Teixeira and Alves, 2010). This means a decrease of approximately two to three orders of magnitude in the perturbation amplitude was achieved in comparison with the results presented in Figure 7. No secondary reflected wave was observed here as well.

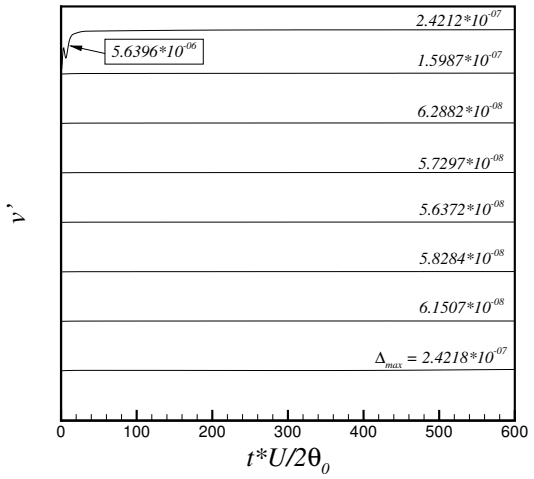

Figure 16. Same as Figure 7, but using an inflow buffer region with $\sigma_0 = 0.1$.

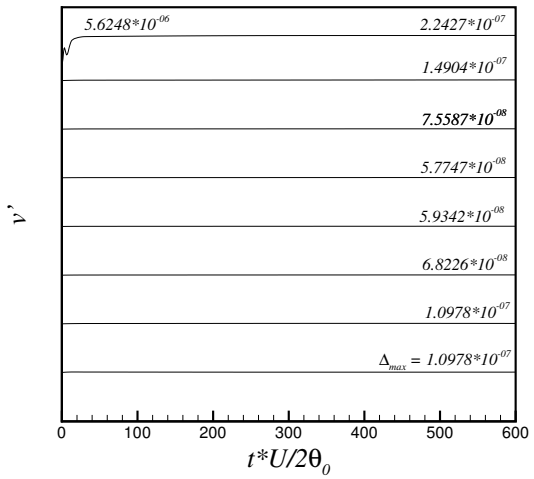

Figure 17. Same as Figure 7, but using an inflow buffer region with $\sigma_0 = 1.0$.

4. CONCLUSIONS

The present paper has shown that inaccurate initial conditions generate substantial error in numerical simulations. Strong evidence was provided to support the idea that their interaction with outflow boundary conditions, and not inflow ones as previously believed, is responsible for the formation of the start-up vortex. Furthermore, the efficacy of global boundary conditions that require reference solutions depend strongly on the accuracy of this solution.

5. ACKNOWLEDGEMENTS

The authors would like to acknowledge the financial support of CAPES/Brazil, Instituto Militar de Engenharia and the Fundação Ricardo Franco.

6. REFERENCES

Blaschak, J.G. and Kriegsmann, G.A., 1988. "A comparative study of absorbing boundary conditions". *Journal of Computational Physics*, Vol. 77, pp. 109–139.

Bodony, D.J., 2006. "An analysis of sponge zones for computational fluid mechanics". *Journal of Computational Physics*, Vol. 212, No. 2, pp. 681–702.

Buell, J.C. and Huerre, P., 1988. "Inflow/outflow boundary conditions and global dynamics of spatial mixing layers". Technical Report N89–24540, Stanford University.

Chomaz, J.M., 2005. "Global instabilities in spatially developing flows: Non-normality and nonlinearity". *Annual Review of Fluid Mechanics*, Vol. 37, pp. 357–392.

Colonius, T., 2004. "Modelling artificial boundary conditions for compressible flow". *Annual Review of Fluid Mechanics*, Vol. 136, pp. 315–345.

Colonius, T. and Lele, S.K., 2004. "Computational aeroacoustics: Progress on nonlinear problems of sound generation". *Progress in Aerospace Sciences*, Vol. 40, pp. 345–416.

Colonius, T., Lele, S.K. and Moin, P., 1993. "Boundary conditions for direct computation of aerodynamic sound generation". *AIAA Journal*, Vol. 31, No. 9, pp. 1574–1582.

Drikakis, D., Grinstein, F.F. and Youngs, D., 2005. "On the computation of instabilities and symmetry-breaking in fluid mechanics". *Progress in Aerospace Sciences*, Vol. 41, pp. 609–641.

Freund, J.B., 1997. "Proposed inflow/outflow boundary condition for direct computation of aerodynamic sound". *AIAA Journal*, Vol. 35, No. 4, pp. 740–742.

Freund, J.B., 2001. "Noise sources in a low-Reynolds-number turbulent jet at Mach 0.9". *Journal of Fluid Mechanics*, Vol. 438, pp. 277–305.

Freund, J.B., Lele, S.K. and Moin, P., 2000. "Direct numerical simulation of a Mach 1.92 turbulent jet and its sound field". *AIAA Journal*, Vol. 38, No. 11, pp. 2023–2031.

Giles, M.B., 1990. "Nonreflecting boundary conditions for euler equation calculations". *AIAA Journal*, Vol. 28, No. 12, pp. 2050–2058.

Grinstein, F.F., 1994. "Open boundary conditions in the simulation of subsonic turbulent shear flows". *Journal of Computational Physics*, Vol. 115, No. 1, pp. 43–55.

Grinstein, F.F. and DeVore, C.R., 2002. "Global instabilities in countercurrent jets". *Physics of Fluids*, Vol. 14, No. 3, pp. 1095–1100.

Grinstein, F.F., Oran, E.S. and Boris, J.P., 1990. "Reinitiation and feedback in global instabilities of subsonic spatially developing mixing layers". *Physical Review Letters*, Vol. 64, No. 8, pp. 870–873.

Grinstein, F.F., Oran, E.S. and Boris, J.P., 1991. "Pressure field, feedback and global instabilities of subsonic spatially developing mixing layers". *Physics of Fluids*, Vol. 3, No. 10, pp. 2401–2409.

Grosch, C.E. and Orszag, S.A., 1977. "Numerical solution of problems in unbounded regions: Coordinate transforms". *Journal of Computational Physics*, Vol. 25, pp. 273–296.

Ho, C.M. and Huerre, P., 1984. "Perturbed free shear layers". *Annual Review of Fluid Mechanics*, Vol. 16, pp. 365–424.

Huerre, P. and Monkewitz, P.A., 1990. "Local and global instabilities in spatially developing flows". *Annual Review of Fluid Mechanics*, Vol. 22, pp. 473–537.

Lardjane, N., Fedioun, I. and Gokalp, I., 2004. "Accurate initial conditions for the direct numerical simulation of temporal compressible binary shear layers with high density ratio". *Computers & Fluids*, Vol. 33, pp. 549–576.

McMullan, W.A., Gao, S. and Coats, C.M., 2007. "A comparative study of inflow conditions for two and three-dimensional spatially developing mixing layers using large eddy simulation". *International Journal for Numerical Menthods in Fluids*, Vol. 255, No. 2, pp. 589–610.

Poinsot, T.J. and Lele, S.K., 1992. "Boundary conditions for direct simulations of compressible viscous flows". *Journal of Computational Physics*, Vol. 101, pp. 104–129.

Tannehill, J.C., Anderson, D.A. and Pletcher, R.H., 1997. *Computational Fluid Mechanics and Heat Transfer*. Taylot & Francis, Philadelphia.

Teixeira, R.S. and Alves, L.S.B., 2010. "A study of initial and boundary conditions for spatially developing planar mixing layers". In *13th Brazilian Congress of Thermal Engineering and Sciences*. Uberlândia, MG, Brazil.

Teixeira, R.S., Alves, L.S.B., Karagozian, A.R. and Kelly, R.E., 2008. "On the solution of the compressible flow equations at small mach numbers". In *12th Brazilian Congress of Thermal Engineering and Sciences*. Belo Horizonte, MG, Brazil.

Thompson, K.W., 1987. "Time dependent boundary conditions for hyperbolic systems". *Journal of Computational Physics*, Vol. 68, No. 1, pp. 1–24.

Wang, M., Freund, J. and Lele, S.K., 2006. "Computational prediction of flow-generated sound". *Annual Review of Fluid Mechanics*, Vol. 38, pp. 483–512.

Wei, M. and Freund, J.B., 2005. "A noise-controlled free shear flow". *Journal of Fluid Mechanics*, Vol. 546, pp. 123–152.

7. RESPONSIBILITY NOTICE

The author(s) is (are) the only responsible for the printed material included in this papers